Out-of-Time-Ordered Correlator's growth rate and Lyapunov Exponent to inspect classical and quantum chaos

July 29, 2021

Cristina Cicali, 1237022, cristina.cicali@studenti.unipd.it
Clelia Corridori, 1230664, clelia.corridori@studenti.unipd.it
Anna Steffinlongo, 1242366, anna.steffinlongo@studenti.unipd.it

Abstract

The aim of this project is to study how chaos arises in quantum systems, how it is quantified and how it is related to the definition of classical chaos, inspecting all these questions focusing on the Kicked Rotor, KR. In particular, we developed a Python code to numerically simulate the temporal evolution of a Gaussian wave-packet whose dynamics is described by the KR Hamiltonian. This lets us compute the OTOC and study its growth rate, the CGR. We also implemented a code to numerically reproduce the classical KR, by using the Chirikov standard map. From this, we computed the Lyapunov Exponent, LE, and the growth rate of the classical version of the OTOC. By comparing these quantities, we will conclude that, since the CGR is more sensitive than the LE to the presence of chaotic islands in the phase space, it could be used to detect local chaos better than global chaos, differently from LE.

Summary

1 Theoretical introduction

Quantum chaos studies the relation existing between classical systems, characterized by a chaotic behavior, and the respective quantum systems. Since it is not possible to use classical arguments such as trajectories in the phase space, it is not possible to study quantum chaos with the same approach as classical chaos. This study can be performed by means of the correspondence principle, indeed it states that classical mechanics is the classical limit of quantum mechanics [3]. In particular, this limit is reached when the dimensionless effective Planck's constant of the system, which is the ratio between the Planck's constant and the system action, tends to zero, $\hbar_{\text{eff}} \to 0$. In this report, we will focus on this semi-classical limit. For this reason, we will consider states represented by Gaussian wave-packets.
The Ehrenfest theorem states that a quantum wave-packet evolution initially follows the classical trajectory having initial momentum and position in the center of the packet. This happens until the wave-packet loses its coherence, at the Ehrenfest time t_E.

A promising approach to tackle this problem is the study of the out-of-time-ordered four-point correlator (OTOC) [9]:

$$C(t) = -\langle [P(t), P(0)]^2 \rangle, \tag{1}$$

where P is the momentum operator at time t and at time 0.
In the semi-classical limit, there exists a quantum chaotic regime at early times where OTOC grows exponentially with a growth rate $\tilde{\lambda}$. The exponential growth of $C(t)$ persists up to the Ehrenfest time, t_E, at which it slows down to a power-law growth with a slowly decreasing power. The Ehrenfest time decreases upon increasing the kicking strength K for fixed $\hbar_{\text{eff}}$. This is consistent with what we can expect since, the greater the kicking strength K, the faster the dynamics.

The growth rate of the OTOC, CGR, appears to be strongly connected to the Lyapunov Exponent, LE. Since the states used to compute the OTOC are Gaussian wave-packets, it is sensitive to the properties of the neighborhood of the center of the Gaussian. This is a key difference with the LE, which is sensitive only to the considered trajectory. For this reason, when computing the OTOC we have to average it on different wave-packets and only then we can extract its growth rate. Instead when computing the Lyapunov Exponent, as we will see in Eq. (3), the average is the last implemented operation. This is a fundamental difference between the two parameters, as we will see in the following sections.

The Lyapunov Exponent characterizes the classical chaotic systems, such as the Kicked Rotor, and determine the rate of exponential separation of initially close trajectories in the phase space. In one-dimensional systems, there is only one positive Lyapunov exponent, $\tilde{\lambda}$, given by the phase-space average of $\lambda(x, p)$:

$$d(t) \approx d(0) e^{\lambda(x,p)t}, \tag{2}$$

with $d(t) = \sqrt{[x'(t) - x(t)]^2 + [p'(t) - p(t)]^2}$ distance at time t between two initially close trajectories in the phase space. Considering the Eq. (2) we can extract the expression for the Lyapunov exponent:

$$\lambda = \Big\langle\!\Big\langle \lambda(x,p) \Big\rangle\!\Big\rangle = \left\langle\!\!\left\langle \lim_{t\to\infty} \lim_{d(0)\to 0} \frac{1}{t} \ln \frac{d(t)}{d(0)} \right\rangle\!\!\right\rangle \tag{3}$$

In this report, we study the Lyapunov exponent and the growth rate of the OTOC for the Kicked Rotor in its classical and quantum version. This system classically presents a transition from regular to chaotic behavior, thus it is optimal to study the correspondence of the LE and the CGR.

1.1 Kicked Rotor

The Kicked Rotor is a simple system that can be studied as a first approximation for more complex ones. For instance, in the semi-classical regime, the Kicked Rotor approximates the behavior of a hydrogen atom in a micro-wave field [6].

The Kicked Rotor for a particle of unitary mass can be described by the Hamiltonian:

$$H(X,P,t) = \frac{P^2}{2} + K\cos(X)\sum_{n=-\infty}^{+\infty}\delta(t-nT), \tag{4}$$

where K is the kicking strength which is a characterizing parameter of the system. For the classical Kicked Rotor, CKR, X and P have to be interpreted as phase space coordinates and for the quantum version, QKR, as operators.

As aforementioned, the classical dynamics of this system undergoes a transition from regular to chaotic as a function of K. In particular, for $K \sim 0$ the system is quasi integrable and in the phase space we can see both regular trajectories and chaotic ones. The number of chaotic trajectories increases while K grows. When $K \sim K_c \sim 0.972$ most of the phase space is occupied by chaotic trajectories, only some islands preserve a regular dynamics. When $K \gg K_c$ all the phase space shows a chaotic behavior. For this reason, we expect the LE to be $\lambda \ll 1$ for $K < 1$ and grows when $K > 1$. This classical dynamics will be inspected more in detail in the following sections and, in particular, in section 2.

The behaviour of the LE can be studied analytically using the Chirikov's formula:

$$\lambda \approx \frac{1}{2\pi}\int_{-\pi}^{\pi}\ln L(x)\,dx, \tag{5}$$

where $L(x) = \left|1 + \frac{K\cos(x)}{2} + \mathrm{sgn}[K\cos(x)]\sqrt{K\cos(x)\left(1+\frac{K\cos(x)}{4}\right)}\right|$. In this report we will compare the results of the numerical simulations with the behaviour of the Eq. (5) for $K \gg 1$ which is:

$$\lambda \approx \ln\left(\frac{K}{2}\right). \tag{6}$$

The quantum Kicked Rotor is characterized by two parameters: in addition to K, presents also in the CKR, there is another important parameter, $\hbar_{\text{eff}}$. This parameter lets us move from the quantum description to the semi-classical limit.
Defining the action as $I = PT$, we can rewrite the commutator $[X, I] = T[X, P] = i\hbar T$. Thanks to this relation we can obtain $\hbar_{\text{eff}} = \hbar T$.

We observe the exponential growth rate of the OTOC for the QKR till the Ehrenfest time. For $K \gtrsim 4$ its behavior is:

$$t_E \sim \frac{|\ln \hbar_{\text{heff}}|}{\ln\frac{K}{2}}. \tag{7}$$

The correlator's growth rate is found to be independent of $\hbar_{\text{eff}}$, and is purely classical at early times [9].

Since the OTOC is highly sensitive to the presence of chaotic islands, we expect the CGR to be greater than the LE. Indeed, as already mentioned, the CGR and the LE are in general two distinct quantities. The difference appears to be more pronounced in the regime of low kicking strength K, where no classical chaos exists globally [9].

The OTOC growth rate can be computed also for the classical Kicked Rotor, $C^{cl}(t)$:

$$C(t) = \hbar_{\text{eff}}^2\left\langle\frac{\delta p(t)^2}{\delta x(0)^2}\right\rangle \approx \hbar_{\text{eff}}^2\left\langle\!\!\left\langle\frac{\Delta p(t)^2}{\Delta x(0)^2}\right\rangle\!\!\right\rangle = C^{cl}(t). \tag{8}$$

where the classical average is computed over the phase space. The relation between $C(t)$ and $C^{cl}(t)$ will be analyzed more in detail in the following sections.

Knowing the behavior of C^{cl},

$$C^{cl}(t) = C^{cl}(1)e^{2\tilde{\lambda}(t-1)}, \tag{9}$$

we can compute the OTOC's exponential growth rate for the CKR:

$$\tilde{\lambda} = \lim_{t\to\infty} \lim_{\Delta x(0)\to 0} \frac{1}{2t} \ln \frac{C^{cl}(t+1)}{C^{cl}(1)}. \tag{10}$$

In the next sections, by using the theory aforementioned, we will analyze the growth of chaos in the classical and quantum KR, focusing on the difference between CGR and LE.

2 Code Development

In this section we focus on the simulations of the dynamics of the quantum Kicked Rotator, and the classical Kicked Rotator, computing the OTOC's growth rate and the Lyapunov exponent for them.
The code for the simulations is organized in three main Jupyter Notebooks:

- *OTOC.ipynb*: This notebook contains the study of the QKR, the computations of its OTOC and the analysis of the latter for different values of the kicking strength, K.
- *OTOCheff.ipynb*: This notebook, similarly to the previous one, contains the study of the QKR, the computations of the OTOC and its analysis, but for different values of the dimensionless effective Planck's constant, $\hbar_{\text{eff}}$.
- *CGRandLE.ipynb*: This notebook contains the analysis, for different values of K, of the following quantities: the growth rate of the OTOC, for the quantum and the classical KR, and the Lyapunov exponent of the classical KR, numerically computed.

There are also two Python files, *OTOCfunc.py* and *CGR_LYAPfunc.py*, containing the useful functions implemented in the Jupyter Notebooks [5].

2.1 OTOC for different values of K

We start from the description of the first notebook. First of all, we set the useful parameters for the simulations of the QKR. We selected the number of points to use for the discretization of the spatial coordinate, N, and, to select the value of the period, T, we considered the relation $2\hbar_{\text{eff}}N \in [2^7; 2^{16}]$ with $\hbar_{\text{eff}} = \hbar T = T$ [9]. Indeed, in our work we always consider $\hbar = 1$. A check to ensure that the parameters N and T respect this condition is implemented. The other useful parameters are the number of kicks, N_{kicks}, the kicking strength, K, and the number of trials over which we want to compute the mean of the OTOC. For each parameter there is a check on its required characteristics (for example sign and type).
To compute the OTOC as in Eq. (1) we need to average over an initial state $|\Psi(0)\rangle$, and we decided to use normalized Gaussian wave-packets in the momentum representation:

$$|\Psi(0)\rangle = \sum_{p=-\infty}^{\infty} a_p^{(0)} |p\rangle \quad \text{with} \quad a_p^{(0)} \sim \exp\left[\frac{(p-p_0)^2}{2\sigma^2}\right], \tag{11}$$

where $\sigma = 4$ and p_0 is randomly selected form a uniform distribution in the range $[-\pi; \pi]$ for each trial in order to explore the phase space. Numerically, we have that $\{|p\rangle\}$, with $p \in [-N; N-1]$, is the finite basis of eigenstates used to represent $|\Psi\rangle$.

To implement the simulation we need to explicit the commutator :

$$\begin{aligned} -[P(t), P(0)]^2 = &+ P(0)P(t)P(t)P(0) + P(t)P(0)P(0)P(t) \\ &- P(t)P(0)P(t)P(0) - P(0)P(t)P(0)P(t). \end{aligned} \tag{12}$$

From this formula we can observe that the temporal evolution of the OTOC is determined by the temporal evolution of the momentum operator P. In the Heisenberg picture we get $P(t) = U^\dagger(t)P(0)U(t)$ with $U(t) = e^{-\frac{i}{\hbar}\hat{H}(t)}$ time evolution operator.

Since we want to compute the OTOC for the QKR, we can observe that its Hamiltonian has a periodic dependency from time, thanks to this we can use the Floquet theory for periodically driven linear systems. The theory for the QKR is further simplified thanks to the fact that we have free propagation alternating with periodic and instant kicks as in Eq. (4).
Therefore, for the QKR the time evolution operator after n periods can be written as

$U(t = nT) = F(T)^n$, with $F(T)$ Floquet operator. This operator depends only on the period T and is composed of two terms, the first one is the kick contribution, U_V, and the second one the free propagation, $U_0(T)$:

$$F(T) = U_V U_0(T) = e^{-ik\cos X} e^{-i\frac{P^2}{2}T}, \tag{13}$$

with P and X momentum and position operators and $k = K/\hbar_{eff}$.

Then we have the time evolution for momentum operator,

$$P(t) = P(nT) = \left[U_0^\dagger U_V^\dagger\right]^n P(0) \left[U_V U_0\right]^n, \tag{14}$$

with $n \in [0; N_{kicks}]$. Considering the Eq. (14) we can discretize the time evolution of the OTOC, $C(nT)$.

The computation of the OTOC, implemented in the function `OTOC`, is performed by means of the expectation value of Eq. (12) on the state $|\Psi(0)\rangle$.

To compute the time evolution of the state in the momentum representation we implemented the function `Ut`. This function applies the Floquet operator to the initial state for a given number of kicks.

All functions of only P are applied in the momentum basis and all functions of only X are applied in the Fourier-transformed representation. The Fourier Transform is computed using the Fast Fourier Transform (FFT) algorithm implemented in the `numpy` package of Python. Here is reported the implementation of the Floquet operator applied to $|\Psi(0)\rangle$, which is indicated as `p_state`.

```
    k=K/T
    # position x discretization
    xmax=2*pi
    dx=xmax/N # step size for the position representation
    xvec=arange(0,xmax,dx) #0=2pi
    x_state=zeros([N],dtype = 'complex_') # state in the position
   representation

    # hamiltonian and temporal evolution
    H0=(dp)**2/2
    V=k*cos(xvec)
    # Floquet components
    U0=exp(-1j*H0*T)
    Uv=exp(-1j*V)

    temp_p=zeros([N],dtype = 'complex_') # Temporary states
    temp_x=zeros([N],dtype = 'complex_')

    for j in range(1,Nkicks+1):
        #Free evolution
        temp_p=U0*p_state
        #AntiFourier
        temp_x=sqrt(N)*fft.ifft(temp_p)
        #Kick
        x_state=Uv*temp_x
        #Fourier
        p_state=(1/sqrt(N)*fft.fft(x_state))
```

Listing 1: Code to implement the Floquet operator applied to the initial state $|\Psi(0)\rangle$.

To reduce the computational time, when calculating the OTOC at different number of kicks $n \in [1, N_{kicks}]$, we used the Parallel function of the Python package `joblib`.

In this notebook, the OTOC is computed for different values of kicking strength, K, and for each of them, it is averaged over a given number of trials.

The resulting averaged OTOC for different values of K is plotted, the analysis of the plot is reported in the section (3).

To analyze the behavior of the OTOC we also computed the quantity:

$$\frac{1}{2t}\ln\left(\frac{C(t)}{C(1)}\right), \tag{15}$$

where $t \in [1, N_{kicks}]$ are the number of kicks, corresponding to the discretized time. Thanks to a plot of Eq.(15) in function of time t in log-log scale, is possible to observe the exponential growth of $C(t)$ as a flat region at early times. Beyond the Ehrenfest time, the exponential growth rate slows down to a power-law growth. The analysis of this plot is reported in the section below.

2.2 OTOC for different values of h_{eff}

In this notebook, we computed again the OTOC, $C(t)$, for a given number of kicks averaged over different trials, but here it is calculated for different values of $\hbar_{\text{eff}} = T$ to observe if the exponential growth rate at early times depends on $\hbar_{\text{eff}}$. As suggested in section (1), we will observe in the following section that it does not depend on $\hbar_{\text{eff}}$.

2.3 Growth rate of the OTOC and Lyapunov exponent for the QKR and the CKR

As observed in section (1) the OTOC's growth rate and the Lyapunov Exponent are two distinct quantities. In this notebook, we want to compute them to study their differences. Therefore, here we computed numerically:

- The growth rate of $C(t)$ for the QKR;
- The Lyapunov exponent for the CKR;
- The growth rate of $C^{cl}(t)$ for the CKR.

Then, we compared them also with the analytical behavior of the Lyapunov exponent for large values of K, as in Eq. (6).

The growth rate of $C(t)$ for the Quantum Kicked Rotor

The strategy suggested by the reference paper to extract the CGR is to determine the times t_E after which, for the different values of K, the exponential growth starts slowing down. Then, it is proposed to fit $C(t)$ from $t = 1$ up to t_E with the function $ae^{2\tilde{\lambda}_{fit}(t-1)}$ to find the parameter $\tilde{\lambda}_{fit}$. Note that $C(0) = 0$, so we can omit $t = 0$.
The problem with this approach is that we are reproducing the results of the paper [9] but with a different value of $\hbar_{\text{eff}}$ for computational resource limits, hence we have smaller values of t_E. This value for high K tends to be $t_E < 3$ and it is impossible to compute a reliable fit over such a small set of points. For completeness, the results of this approach are reported in [5].

Using a different approach, we decided to consider the classical correspondence of $C(t)$ for the time interval in which we are interested, $t < t_E$ [7]:

$$C(t) \approx C^{cl}(t) = \hbar_{\text{eff}}^2 \left\langle\!\!\left\langle \frac{\Delta p(t)^2}{\Delta x(0)^2} \right\rangle\!\!\right\rangle, \tag{16}$$

with the average computed over the phase space. Thanks to this approach, knowing the behaviour of C^{cl} from Eq. (9), we can compute the OTOC's exponential growth rate, starting from Eq. 10 and using $2\tilde{\lambda} = \ln\frac{C(t)}{C(t-1)}$. Recalling that $C(0) = 0$ we considered $t > 0$.

The following figure shows an example of the computation of $\tilde{\lambda}(t)$ for $K = 0.045$, plotting $2\tilde{\lambda}(t)$ as a function of N_{kicks}. Here it is possible to observe that, after the initial kicks, $\tilde{\lambda}(t)$ is

almost constant till t_E. In this region, we fitted $2\tilde{\lambda}(t)$ with $y = constant$. We repeated the fitting procedure for a given number of trials and then we averaged over them.

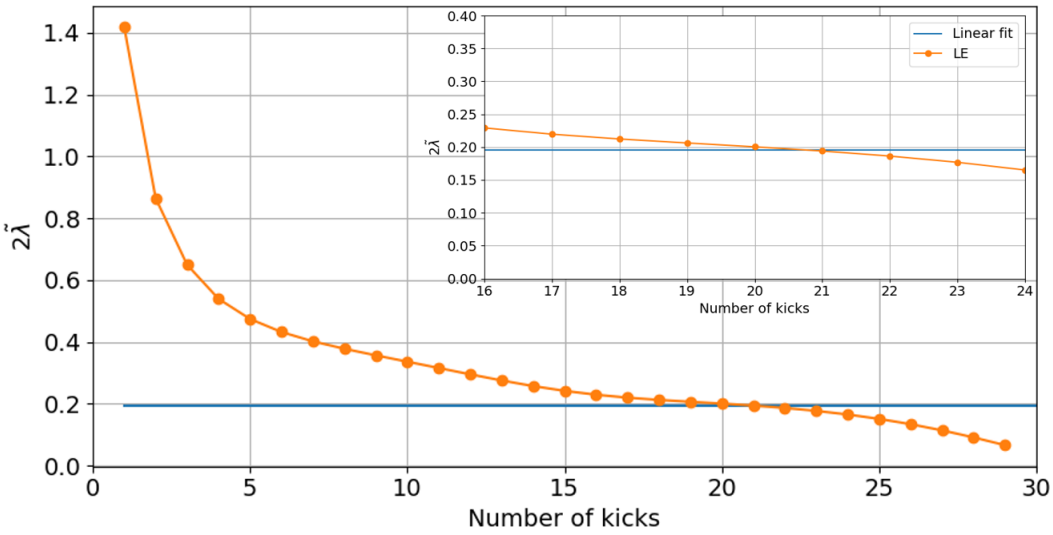

Figure 1: $2\tilde{\lambda}(t)$ as a function of the number of kicks, t, for $K = 0.045$ and fit $y = constant$ in the region $t \in [16, 24]$.

Thanks to this approach we computed the CGR for the QKR for different values of K. Also for this method the size of the flat region for $K \gg 1$ has a time size of $N_{kicks} < 3$ but it is more precise than the previous one. The comparison between the two methods is shown in [5].

The Lyapunov exponent for the Classical Kicked Rotor

We described the expression for the time evolution of the distance at time t, $d(t)$, between two initially close trajectories, $d(0) \ll 1$, in the phase space in Eq. (2).
The equation Eq. (3) can be used directly to compute the Lyapunov exponent of CKR, which is calculated knowing the initial position and momentum, x_0 and p_0, and the distance $d(t)$. To compute the last one quantity we started considering two trajectories that obey to the Chirikov standard map [4]:

$$\begin{cases} p_{n+1} \overset{\text{mod } 2\pi}{=} p_n + K \sin x_n \\ x_{n+1} = x_n + p_{n+1} \end{cases}, \tag{17}$$

$$\begin{cases} p'_{n+1} \overset{\text{mod } 2\pi}{=} p'_n + K \sin x'_n \\ x'_{n+1} = x'_n + p'_{n+1} \end{cases}, \tag{18}$$

with $n \in [0, N_{kicks}]$.

Then, we introduced the relative coordinates ξ_n and η_n, such that $\boldsymbol{d}(n) = \begin{pmatrix} \eta_n \\ \xi_n \end{pmatrix}$. The length of $\boldsymbol{d}(n)$ is the distance between two trajectories in the phase space at step n.

It is possible to compute the standard map for ξ_n and η_n:

$$\begin{cases} \eta_{n+1} = \eta_n + K(\sin x'_n - \sin x_n) \\ \xi_{n+1} = \xi_n + \eta_{n+1} \end{cases}. \tag{19}$$

Then, by using a trigonometric identity, we can rewrite:

$$\sin x'_n - \sin x_n = \sin x_n(\cos \xi_n - 1) + \sin \xi_n \cos x_n = \xi_n \cos x_n. \tag{20}$$

The last equality is obtained considering the linear order of ξ_n, with $\xi_n \ll 1$. Now, the mapping tangent to that in Eq. (19) is given by the expression:

$$\begin{cases} \eta_{n+1} = \eta_n + (K \cos x_n)\xi_n \\ \xi_{n+1} = \xi_n + \eta_{n+1} \end{cases} . \tag{21}$$

We need to notice that the Eq. (21) contains x_n, therefore, for the numerical simulation we need to propagate the standard map (Eq. 17) and tangent map (Eq. 21) using the values of x_n from the former equation as inputs for the latter.

In the code implementation of Eq. (3), due to the overflow of $\boldsymbol{d}(t)$ caused by the exponential stretching, we implemented the Benettin algorithm [1]: we selected an initial $\boldsymbol{d}(0)$ with unitary norm and a random set of initial conditions (x_0, p_0), we propagated the standard map (Eq. 17) and the tangent map (Eq. 21) for N_{kicks}. After N_{kicks} iterations we saved $\boldsymbol{d}(N_{kicks})$ and normalized it to have unitary norm, dividing it by $d(t) = \|\boldsymbol{d}(t)\|$.
We repeated this procedure for a given number of times, M, each time considering the final normalized $\boldsymbol{d}(iN_{kicks})$ and the final coordinates, $(x(iN_{kicks}), p(iN_{kicks}))$, with $i = 1, ..., M$, as initial conditions. This way we obtained a set of distances $\{d(iN_{kicks})\}$.

Given an initial point (x_0, p_0) is then possible to compute the Lyapunov Exponent for a given K using the numerical implementation of the Eq. (3):

$$\lambda(x_0, p_0) = \frac{1}{MN_{kicks}} \sum_{t=1}^{N_{kicks}} \ln d(t). \tag{22}$$

We chose N_{kicks} as large as possible avoiding the overflow. Then, $\lambda(x_0, p_0)$ has to be averaged over the phase space, this is implemented computing it for a set of initial conditions $\{(x_{0,i}, p_{0,i})\}_{i=1,...,Ntrials}$ uniformly distributed in the interval $[0, 2\pi]$.

The growth rate of $C^{cl}(t)$ for the Classical Kicked Rotator

Using the Eq. (9) we can compute the growth rate of $C^{cl}(t)$ for the CKR, averaged over some interval in time to improve the accuracy:

$$\widetilde{\lambda} = \frac{1}{2(t_c - 1)} \sum_{t=2}^{t_c} \ln \frac{C^{cl}}{C^{cl}(t-1)}, \tag{23}$$

where t_c is selected such that the overflow is prevented. Indeed, this time is not possible to rescale $\boldsymbol{d}(t)$, because this would alter the expression for the CGR.
Substituting in the equation above $C^{cl}(t)$ from Eq. (9) and considering $\Delta x(0)$ constant throughout the phase space, we obtain the expression to compute numerically the growth rate of $C^{cl}(t)$:

$$\widetilde{\lambda} = \frac{1}{2(t_c - 1)} \sum_{t=2}^{t_c} \ln \frac{\left\langle\!\left\langle [\Delta p(t)]^2 \right\rangle\!\right\rangle}{\left\langle\!\left\langle [\Delta p(t-1)]^2 \right\rangle\!\right\rangle}, \tag{24}$$

where $\Delta p(t) = \eta(t)$ is computed using the tangent map.

Once all the quantities described above are computed we plot them to analyze their behavior and compare them, as described in the next section.

3 Results

To analyze in detail the reference paper [9], we now present the results obtained implementing the code described in section (2).
The classical Kicked Rotor, without any perturbation, has stable trajectories [4]. When adding a sinusoidal perturbation to the system, namely the kick contribution in the Hamiltonian (Eq. 4), it is possible to observe a transition to chaos increasing the value of K, as described in section (1). We observed this transition numerically by means of the Chirikov standard map. In the following figure we report the trajectories in the phase space, obtained by using the previous map for different values of K.

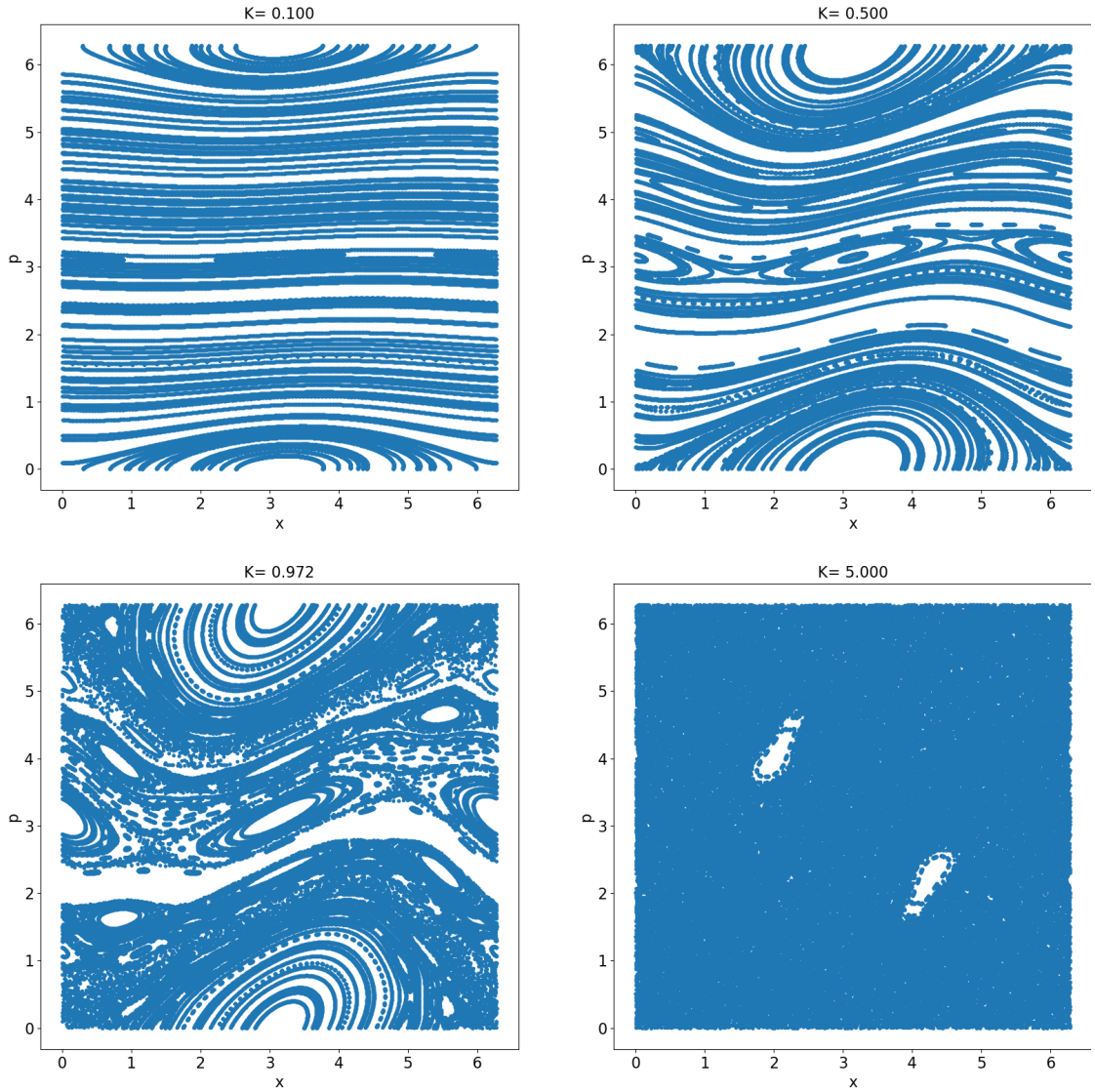

Figure 2: Classical KR trajectories in the phase space in the interval $[0, 2\pi]$ for different values of $K = [0.1, 0.5, 0.972, 5]$. We considered 100 trajectories and $N_{kicks} = 1000$. In the plots it is possible to observe the transition to chaos increasing K. The critical value is $K_c \sim 0.972$.

In the first plot, $K = 0.1$, we observe mostly regular trajectories. In the second plot, $K = 0.5$, there are both regular and chaotic trajectories. The third plot, $K \sim K_c = 0.972$, presents the transition to chaos and the destruction of all regular trajectories that separate the phase space. There still exists some islands in which are possibles regular trajectories,

surrounded by an increasing number of chaos trajectories. Instead, in the last plot with $K = 5$, the phase space is completely occupied by chaotic trajectories: the particle during the trajectory can visit each point of the phase space creating a diffusive behavior.

Considering the quantum KR, it is possible to compute numerically the evolution of the probability density related to the Gaussian state (Eq. 11). For a kicking strength of $K = 5$, the wave packet spreads completely after few kicks. Indeed in Fig. 3 we show that the spreading is present for $N_{kicks} = 4$. To better illustrate the spreading we chose $N = 2^{10}$ and $T = 2^{-4}$, those respect the condition $2TN \in [2^7, 2^{16}]$. The wave functions in both the representations are normalized and there is a check to ensure the correct normalization with a tolerance of 10^{-4}.

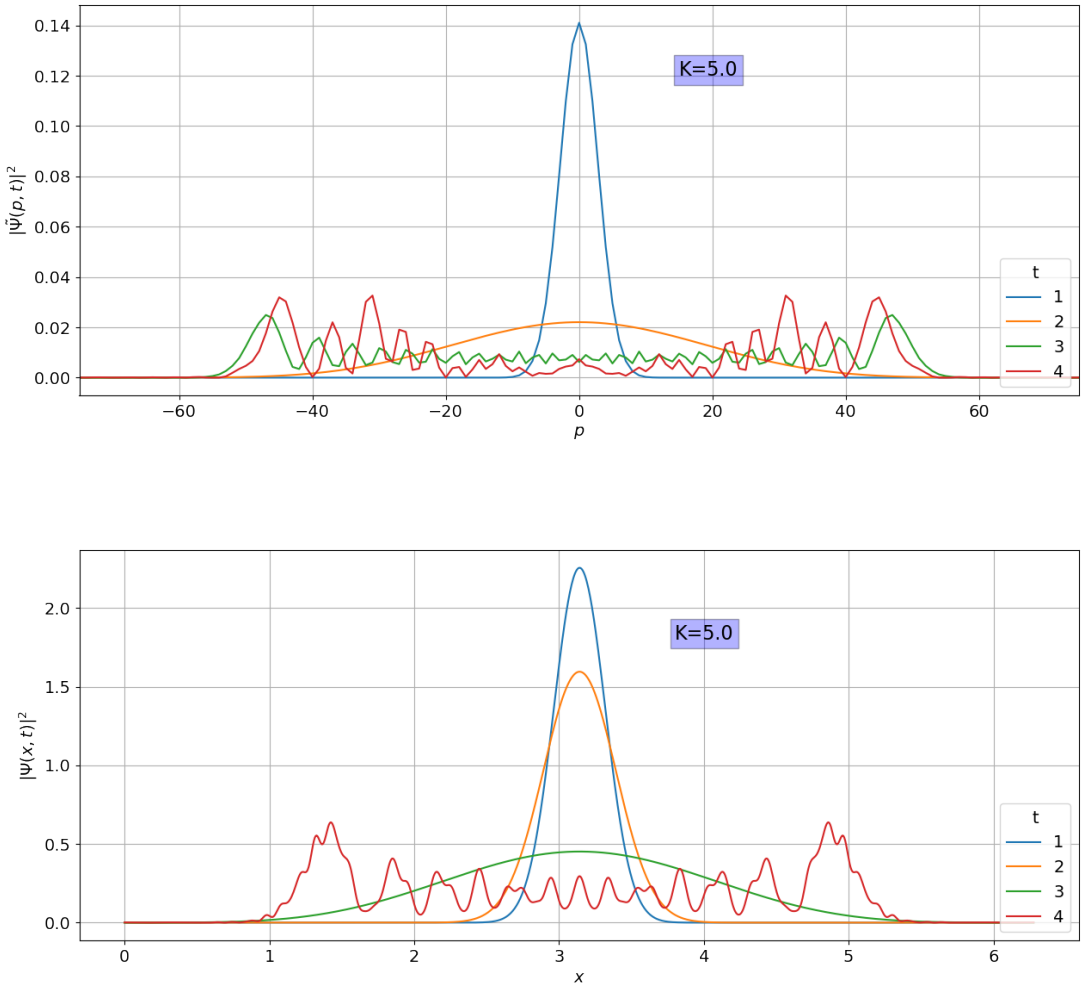

Figure 3: Spreading of $|\Psi(0)\rangle$ for $K = 5$. In the first plot $|\Psi(t)\rangle$ is in P-representation. In the second one it is in X-representation. $N = 2^{10}$ and $T = 2^{-4}$.

3.1 The OTOC

Here we describe the results of the OTOC computation for the QKR, both for different values of the kicking strength K and for different values of $\hbar_{\text{eff}}$, as reported in the sections (2.1) and (2.2).

OTOC for different values of K

The OTOC, $C(t)$, is computed as function of the number of kicks for $K = [0.5, 2, 3, 4, 6, 10]$. As parameters to compute the OTOC we have chosen $N = 2^{14}$ and $T = 2^{-7}$, considering the

condition $2TN \in [2^7, 2^{16}]$. The number of kicks are $N_{kicks} = 100$ and the average is performed over 50 trials.

In figure 4 is possible observe how $C(t)$, related to the smallest value of K, fluctuates in time. These oscillations could be due to the fact that for $K < 1$ already exist some chaotic islands and the OTOC behaviour is affected by the proximity to these.
The exponential growth of $C(t)$ in log scale is represented by the linear growth in the number of kicks till t_E, as suggest also from the spreading of the wave-packet [2] [8].

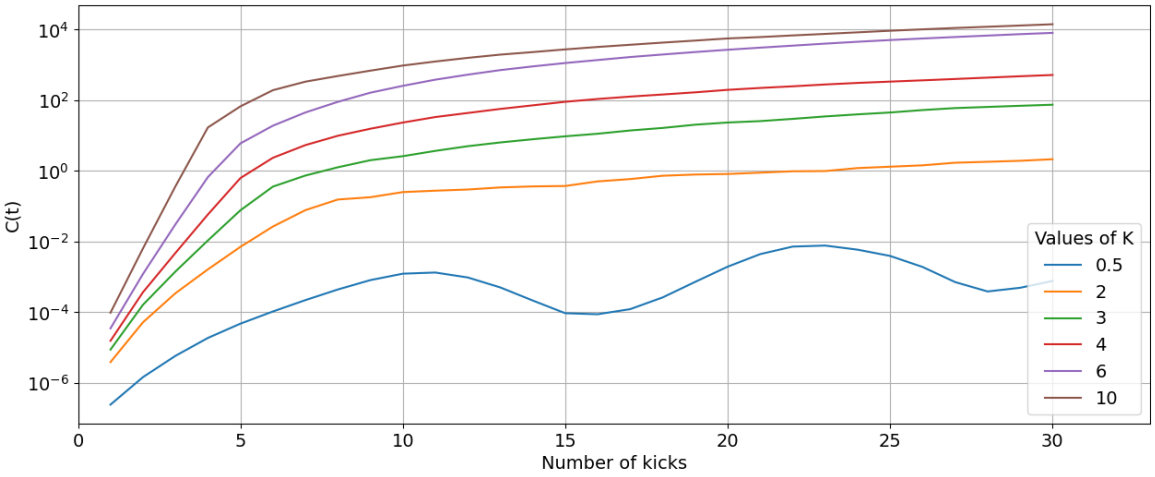

Figure 4: $C(t)$ as function of N_{kicks} for kicking strength $K = [0.5, 2, 3, 4, 6, 10]$ and $\hbar_{\text{eff}} = 10^{-7}$. In the plot the y axis is in log scale.

To deeply study the OTOC behaviour, we computed $\ln[C(t)]/2t$, after having normalized $C(t)$ to $C(1)$ as in Eq. (15). In Fig. 5 it is possible to observe a constant behavior before the Ehrenfest time, which corresponds to the exponential growth of $C(t)$. Beyond t_E the behavior is reduced to a power-law growth with a decreasing power [9].

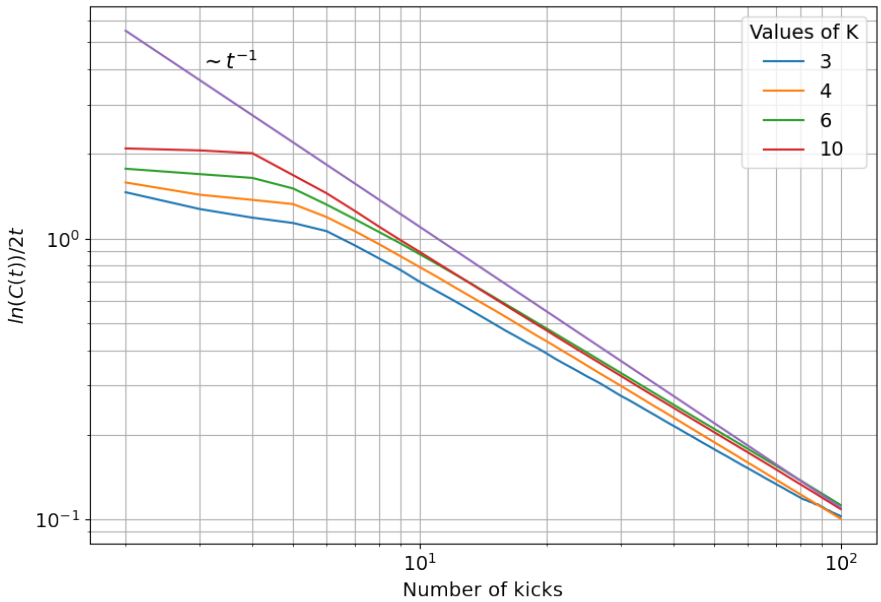

Figure 5: Log-log scale plot of $\ln[C(t)]/2t$ as function of N_{kicks} for $K = [0.5, 2, 3, 4, 6, 10]$ and $\hbar_{\text{eff}} = 2^{-7}$. In the plot is shown also the asymptotic behaviour, t^{-1}.

We also notice that the smaller K, the bigger t_E, as expected from figure 4 and described in section (1).

From the flat region at early times, before t_E, we can obtain an estimate of the exponential growth rate of $C(t)$, the CGR. This will be the focus of our study in subsection (3.2).

The Ehrenfest time is consistent with the behaviour $t_E \sim \frac{|\ln(\hbar_{\text{eff}})|}{\ln(K/2)}$, indeed $t_E(K=10) \sim 4$ and $t_E(K=6) \sim 5$. Moreover, these values are consistent with the t_E that we can estimate from Fig. 5. Since for $K \lesssim 4$ we do not observe a completely flat region it is not possible to estimate t_E, as suggested in the reference paper. This could be due to some residual islands of order in the phase space for small values of K.

OTOC for different values of $\hbar_{\text{eff}}$

To further study the exponential growth, we computed the OTOC for $\hbar_{\text{eff}} = [2^{-2}, 2^{-4}, 2^{-6}, 2^{-8}]$ and $K = 4$. In Fig. 6 we observe that the bigger is the value of the dimensionless effective Planck's constant, the smaller is the interval in which we observe the exponential growth. As we will see in Fig. 7, the exponential growth rate looks similar for each value of $\hbar_{\text{eff}}$.

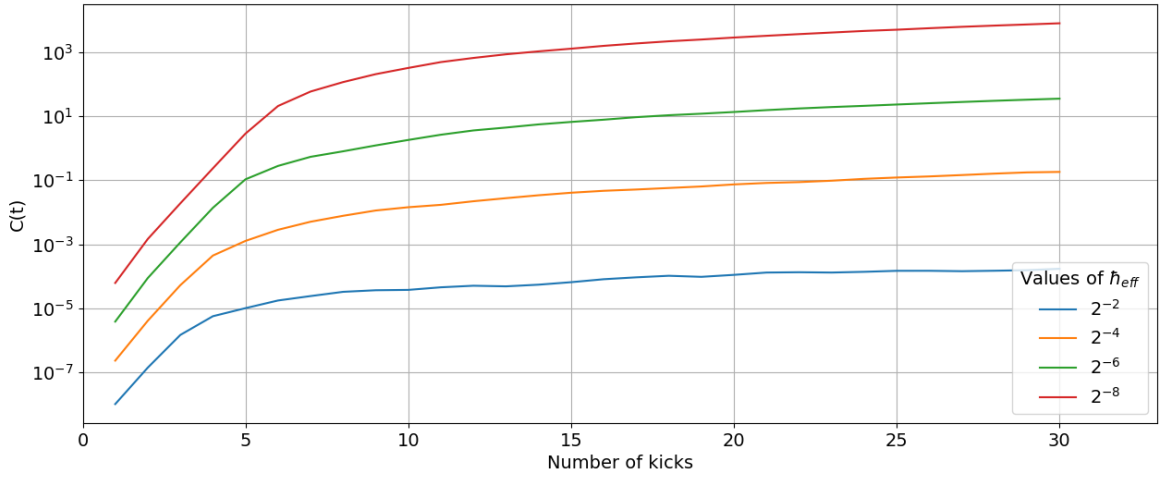

Figure 6: $C(t)$ as function of the number of kicks for $\hbar_{\text{eff}}$=$[2^{-2}, 2^{-4}, 2^{-6}, 2^{-8}]$ and K=4. In the plot the y axis is in log scale.

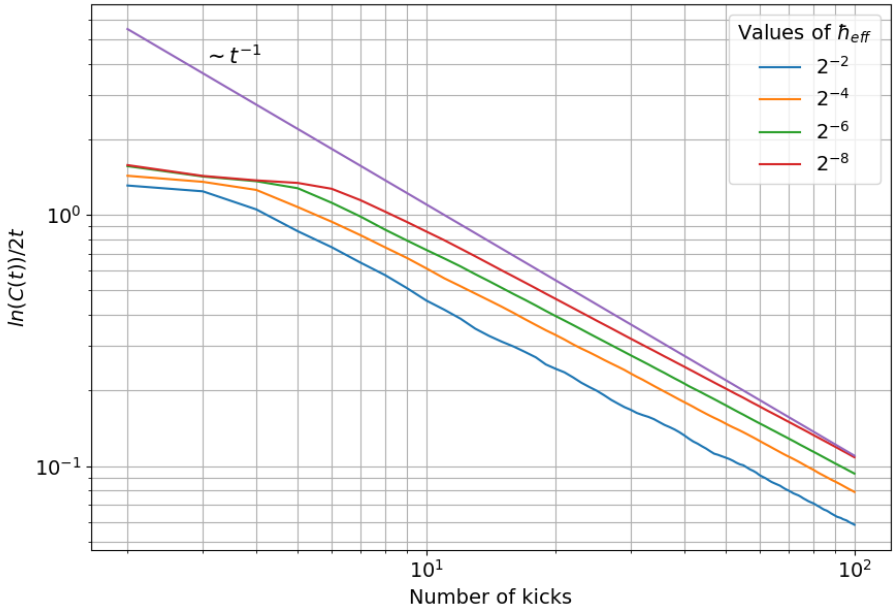

Figure 7: Log-log scale plot of $\ln[C(t)]/2t$ as function of N_{kicks} for $\hbar_{\text{eff}}$=$[2^{-2}, 2^{-4}, 2^{-6}, 2^{-8}]$ and $K = 4$. In the plot is shown also the asymptotic behaviour, t^{-1}.

As done for different values of K, we computed the quantity in Eq.(15) and the results can be observed in Fig. 7.

First of all, the rate of the exponential growth is almost the same for different values of $\hbar_{\text{eff}}$. This suggest that the CGR values are independent from $\hbar_{\text{eff}}$. The Ehrenfest time depends on $\hbar_{\text{eff}}$ and is consistent with the expected behaviour, indeed $t_E(\hbar_{\text{eff}} = 2^{-2}) \sim 3$, $t_E(\hbar_{\text{eff}} = 2^{-4}) \sim 4$, $t_E(\hbar_{\text{eff}} = 2^{-6}) \sim 5$ and $t_E(\hbar_{\text{eff}} = 2^{-8}) \sim 6$.

3.2 Comparison between Classical and Quantum Chaos

As described previously, here we focus on the second part of this work, the comparison between classical and quantum chaos. Therefore, we computed numerically the values of the OTOC's growth rate both for the quantum and the classical KR and the values of the Lyapunov exponent for the classical KR, using the procedure describe in 2.3.
Here we define the parameters used for the computation. We chose 50 values of K equally spaced in log-scale in the interval $[10^{-2}, 10^{2}]$ for every computation, and then we set the specific values for each one:

- *CGR for the quantum KR*: $\hbar_{\text{eff}} = 2^{-7}$, $N = 2^{14}$, $N_{kicks} = 30$, number of trials to average $C(t)$ $N_{trials,OTOC} = 10$, number of trials to average the CGR $N_{trials,CGR} = 10$;
- *LE for the classical KR*: to compute the Eq. (22) we selected $M = 1000$, $N_{kicks} = 50$ and the number of trials to average the LE $N_{trials} = 100$;
- *CGR for the classical KR*: to compute the Eq. (24) we selected $N_{kicks} = t_c = 50$ and the number of trials to average the LE $N_{trials} = 1000$;

The values of N_{kicks} for the last two computations are set to avoid the overflow.

In the figure 8 is presented the comparison between the quantities listed above.

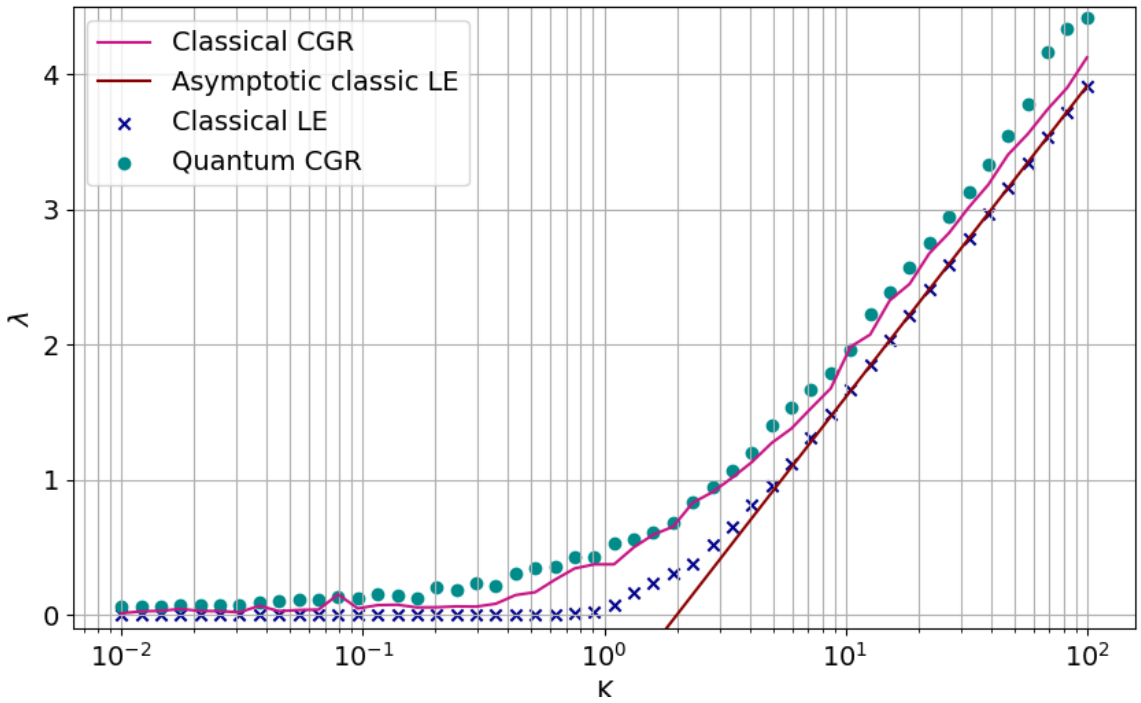

Figure 8: Comparison between CGR for quantum and classical KR, and LE for the classical one. Also the analytical behaviour of LE is considered. The used parameters are the ones listed above.

Firstly, the last values of the quantum CGR, $K > 60$, do not behave as expected in [9], because we are computing the linear fit for $t < t_E$, with $t_E < 3$, as already discussed.

From Fig. 8 we also observe that, except for some fluctuations probably due to the low number of trials, the behavior of the CGR for the classical KR is similar to the quantum one. The low number of trials could not be improved because of the lack of computational power.

The relative differences between the two quantities are highlighted in Fig. 9. After the initial values of K, the difference between the CGRs stabilizes below the 10%, thus we can confirm that they have similar behavior. As for the first values of K, $K \lesssim 4$, the relative difference is high. This could be due to the CGR fluctuations we already talked about in the comment of Fig. 5.

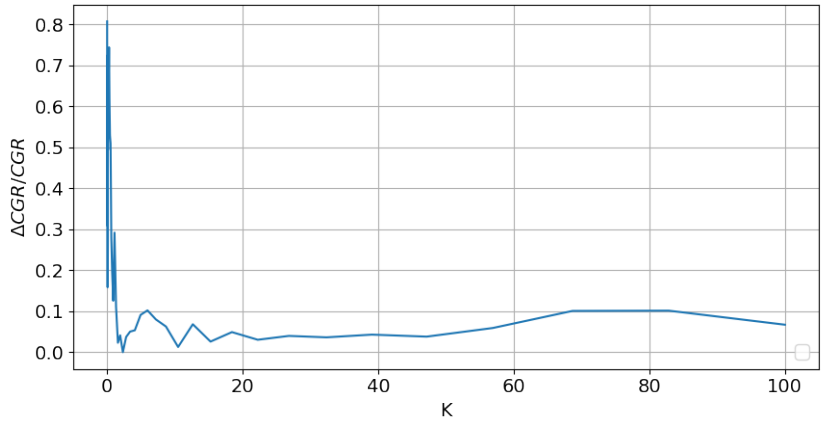

Figure 9: Differences between the classical and the quantum CGR divided by the values of the CGR of the quantum kicked rotor.

We also observe that the Lyapunov Exponents agree with their asymptotic values, computed as $\ln(K/2)$ from the Eq. (5) for high values of K, $K > 8$. This agreement is better shown in Fig. 10, where we have shown the ratio between the difference between these quantities and the analytical value of LE.

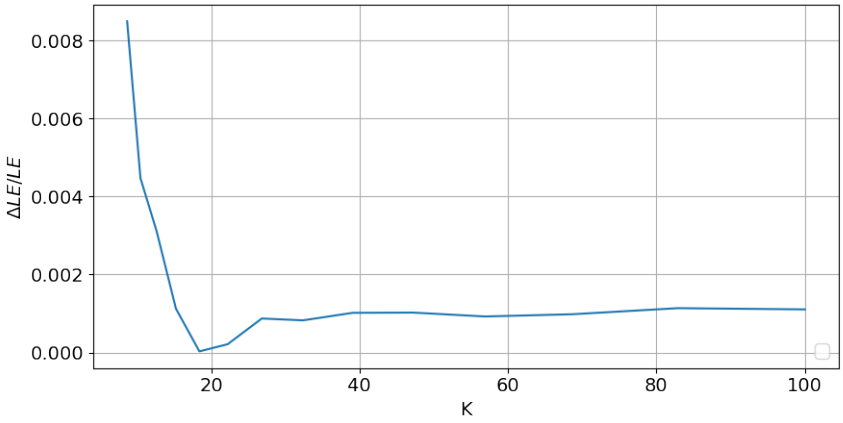

Figure 10: Differences between numerical and analytical LE, divided by the values of the analytical behavior for $K > 8$.

In Fig. 8 for low kicking strength K, where no classical chaos exists globally, the LE quickly decreases, while the OTOC's growth rate may decrease much slower showing higher sensitivity

to small chaotic islands in the phase space. Computing the difference between the LE and the quantum CGR we can observe in Fig. 11 that it stabilize for high values of K, $K \gtrsim 15$. We attribute this difference primarily to the order of averaging that changes in the CGR and LE calculations.
For $K > 60$ it is not possible to compare them because the values of the quantum CGR are not reliable, due to the fitting procedure described in section (2.3).

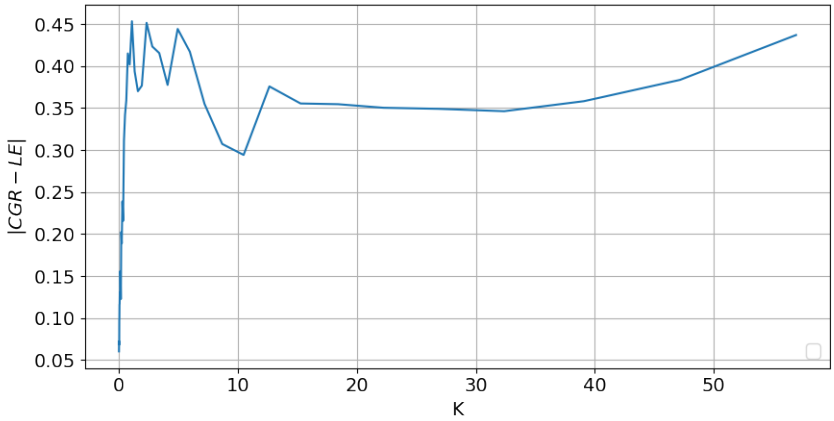

Figure 11: Absolute differences between classical LE and quantum CGR.

Both the quantum and the classical CGR significantly exceed LE. This can suggest that the CGR may not be a useful quantity to discriminate between classically regular and chaotic dynamics globally. Instead, thanks to its sensitivity to chaos islands, it can be used to detect them.

4 Conclusion

In this report we had the possibility to deeply inspect the out-of-time-ordered four-point correlator, OTOC, that may serve as a useful characteristic of quantum-chaotic behavior. We have studied it for the classical and quantum versions of the Kicked Rotor which is a simple system that presents both classical and quantum chaos. Moreover, it represents a powerful tool to study more complex systems.

We also compared OTOC's growth rate at early times with the standard definition of the classical Lyapunov exponent. This comparison helps us to understand whether the OTOC is a suitable parameter to study quantum chaos. Using both quantum and classical numerical simulation, we observed that the CGR and the LE are in general distinct quantities. As matter of fact, this is because the order of the logarithm and average operations are exchanged in the CGR and in the LE.

All the results presented in this report are computed to deeply study the arguments proposed in the reference paper [9]. Due to a lack of computational power, we could not use the same parameters for each case scenario. Therefore, we decided to use different parameters still respecting the same conditions. This led us to analogous results, with the same behavior, but not always the same values and more fluctuations. To remove these fluctuations, it is recommended to compute the average over more trials. To obtain the same values, instead, it would be necessary to use the same parameters, and this could improve also the fitting procedure.

The OTOC growth rate exponents for the classical and quantum Kicked Rotor agree. Moreover, for high values of K both classical and quantum CGRs significantly exceed LE. This is because, as already observed, the CGR is highly sensitive to chaotic islands, thus it could be a powerful tool to detect them in the phase space but not to detect global chaos.

All the implemented scripts are available on GitHub ([5]).

References

[1] Giancarlo Benettin et al. "Lyapunov Characteristic Exponents for smooth dynamical systems and for Hamiltonian systems; A method for computing all of them. Part 2: Numerical application". In: *Meccanica* 15 (Mar. 1980), pp. 21–30. DOI: 10.1007/BF02128237.

[2] Gennady P Berman and George M Zaslavsky. "Condition of stochasticity in quantum nonlinear systems". In: *Physica A: Statistical Mechanics and its Applications* 91.3-4 (1978), pp. 450–460.

[3] Giulio Casati et al. "Stochastic behavior of a quantum pendulum under a periodic perturbation". In: *Stochastic behavior in classical and quantum Hamiltonian systems*. Springer, 1979, pp. 334–352.

[4] Boris V Chirikov. "A universal instability of many-dimensional oscillator systems". In: *Physics Reports* 52.5 (1979), pp. 263–379. ISSN: 0370-1573. DOI: https://doi.org/10.1016/0370-1573(79)90023-1. URL: https://www.sciencedirect.com/science/article/pii/0370157379900231.

[5] Clelia Corridori Cristina Cicali and Anna Steffinlongo. *Out-of-Time-Ordered Correlator's growth rate and Lyapunov Exponent to inspect classical and quantum chaos*. 2021. URL: %5Curl%7Bhttps://github.com/CleliaCorridori/QuantumInformation_project%7D.

[6] P.M. Koch and K.A.H. van Leeuwen. "The importance of resonances in microwave "ionization" of excited hydrogen atoms". In: *Physics Reports* 255.5 (1995), pp. 289–403. ISSN: 0370-1573. DOI: https://doi.org/10.1016/0370-1573(94)00093-I. URL: https://www.sciencedirect.com/science/article/pii/037015739400093I.

[7] A. I. Larkin and Yu. N. Ovchinnikov. "Quasiclassical Method in the Theory of Superconductivity". In: *Soviet Journal of Experimental and Theoretical Physics* 28 (June 1969), p. 1200.

[8] Juan Maldacena, Stephen H Shenker, and Douglas Stanford. "A bound on chaos". In: *Journal of High Energy Physics* 2016.8 (2016), pp. 1–17.

[9] Efim B Rozenbaum, Sriram Ganeshan, and Victor Galitski. "Lyapunov exponent and out-of-time-ordered correlator's growth rate in a chaotic system". In: *Physical review letters* 118.8 (2017), p. 086801.